Thin Solid Films 552 (2014) 232–240

Contents lists available at ScienceDirect

Thin Solid Films

journal homepage: www.elsevier.com/locate/tsf

Decomposition of amorphous Si_2C by thermal annealing

R. Gustus [a,b,c], W. Gruber [b], L. Wegewitz [a,d], U. Geckle [e], R. Prang [f], C. Kübel [f], H. Schmidt [b,d], W. Maus-Friedrichs [a,d,*]

[a] Institut für Energieforschung und Physikalische Technologien, Technische Universität Clausthal, Leibnizstrasse 4, 38678 Clausthal-Zellerfeld, Germany
[b] Institut für Metallurgie, Technische Universität Clausthal, Robert-Koch-Str. 42, 38678 Clausthal-Zellerfeld, Germany
[c] Institut für Elektrochemie, Technische Universität Clausthal, Arnold-Sommerfeld-Straße 6, 38678 Clausthal-Zellerfeld, Germany
[d] Clausthaler Zentrum für Materialtechnik, Technische Universität Clausthal, Leibnizstrasse 4, 38678 Clausthal-Zellerfeld, Germany
[e] Karlsruher Institut für Technologie, Institute for Applied Materials, Eggenstein-Leopoldshafen, Germany
[f] Karlsruher Institut für Technologie, Institute of Nanotechnology and Karlsruher Micro Nano Facility, Eggenstein-Leopoldshafen, Germany

ARTICLE INFO

Article history:
Received 29 April 2013
Received in revised form 16 December 2013
Accepted 17 December 2013
Available online 27 December 2013

Keywords:
Silicon carbide
Silicon
Amorphous films
Crystallization
Sputter deposition

ABSTRACT

In the present paper, the decomposition and the crystallization behaviour of amorphous Si_2C films, which were deposited by r.f. magnetron co-sputtering on Si wafer substrates, are investigated. For analysis, the following methods were used: x-ray photoelectron spectroscopy (XPS), transmission electron microscopy (TEM), grazing incidence x-ray diffractometry (GIXRD), atomic force microscopy and scanning electron microscopy. After deposition, the films exhibited a homogenous amorphous structure with a variety of bonding states reaching from homonuclear silicon-like Si-Si bonds over mixed Si-Si-C bonds to heteronuclear Si-C bonds. Annealing at 1200 °C for 2 h leads to the crystallization of silicon and silicon carbide with grain diameters of several nanometers within the amorphous matrix, as evidenced by GIXRD and TEM. With XPS also a distinct change of the bonding states is detected. After 2 h of annealing, only Si-Si and Si-C bonds are detectable. After prolonged annealing at 1200 °C for 20 h, XPS shows only Si-C bonding states but no more Si-Si bonding. In addition, GIXRD verifies the absence of any polycrystalline silicon in the film. The microstructure of the film changed dramatically towards a jagged and porous structure. The vanishing of silicon during isothermal annealing is explained on base of in situ and ex situ TEM measurements, and a possible model for decomposition is suggested.

© 2013 Elsevier B.V. All rights reserved.

1. Introduction

Thin films of non-stoichiometric silicon carbide ($Si_{1-x}C_x$) are interesting for applications in various branches of technology. Typical examples are window layers in solar cells [1], insulating layers in thin film transistors [2], thin film light emitting diodes [3,4], colour displays [5], UV detectors [6], Li ion battery anodes [7] and microelectromechanical systems (MEMS) [8]. An actual field of research is the tailored synthesis of silicon nano crystals embedded in an amorphous matrix of silicon carbide for application as tandem solar cells [9,10]. For such a design, a fundamental understanding of the amorphous to crystalline transition is of large importance, especially for Si-rich films of composition $Si_{1-x}C_x$ ($x < 0.5$).

Besides an investigation of phase formation, phase separation and crystallization kinetics, the understanding of the chemical order of the amorphous system as well as the early stages of crystallite formation are of importance. As illustrated in the tetrahedron model of Ref. [11], for amorphous silicon–carbon alloys, three types of chemical order have to be considered: (a) complete random order where no preferential chemical bonding between Si and C atoms exists; (b) complete chemical order, which means that in Si-rich alloys a C atom in the centre of a tetrahedron is surrounded by four Si atoms and that a maximum of possible Si–C bonds is realised; and (c) complete chemical order with phase separation, which means that the Si–C bonds are clustered [11]. According to molecular dynamics simulations [12], about 40–45% homonuclear bonds might be present in stoichiometric amorphous silicon carbide. However, the same simulations also revealed a high degree of short- and medium-range order excluding a complete random order.

In a recent study [13], we investigated the thermal stability of thin films of Si_2C at 800 °C under Ultra High Vacuum (UHV) conditions. In this work, the formation of Si crystals with diameters of about 500 nm on the surface of the film was observed. Besides, no significant amount of crystallized SiC was detected by grazing incidence x-ray diffractometry (GIXRD). Further investigations [14] of the crystallization kinetics of amorphous Si_2C films by GIXRD at temperatures between 1200 °C and 1350 °C revealed a transient formation of crystalline Si, superimposed by stoichiometric SiC crystallization.

In this study, we focussed on the processes determining the thermal stability of amorphous Si_2C at 1200 °C. Therefore, microstructure and chemical bonds in the films are investigated at different time scales of annealing by means of x-ray photoelectron spectroscopy (XPS),

* Corresponding author at: Institut für Energieforschung und Physikalische Technologien, Technische Universität Clausthal, Leibnizstrasse 4, 38678 Clausthal-Zellerfeld, Germany.
E-mail address: w.maus-friedrichs@pe.tu-clausthal.de (W. Maus-Friedrichs).

0040-6090/$ – see front matter © 2013 Elsevier B.V. All rights reserved.
http://dx.doi.org/10.1016/j.tsf.2013.12.033

ex situ and in situ transmission electron microscopy (TEM), grazing incidence x-ray diffractometry (GIXRD), atomic force microscopy (AFM) and scanning electron microscopy (SEM).

2. Experimental details

Thin amorphous films of non-stoichiometric silicon carbide (Si_2C) were prepared by a r.f. co-sputtering technique using a 3″ ION'X planar magnetron source (TFC, Grafenberg, Germany) mounted on a standard DN 150 CF double cross recipient equipped with pre-sputter shutter and sample positioner allowing various distances (100–200 mm) between magnetron and substrate. Deposition was done at a rate of 5 nm/min, using argon (6.0) sputter gas at an operating pressure of 0.1 Pa, a sputtering power of 80 W and a substrate temperature of 200 °C. Carbon stripes (99.99%; Goodfellow, Bad Nauheim, Germany) of 5 mm × 25 mm were radially fixed at equal distances on a silicon base target (99.999%; Norwegian Talc, Bad Soden, Germany). The target size was 3″, giving a power density of 1.76 W/cm^2. The films were deposited on silicon (100) wafers (Si-Mat Silicon Materials). Measurements with Rutherford backscattering spectrometry revealed a Si:C ratio of 2:1 [14]. The films were annealed in a resistance tube (Al_2O_3) furnace under argon atmosphere (99.996%) at a pressure of 10^5 Pa and a temperature of 1200 °C for 2 and 20 h, respectively.

X-ray photoelectron spectroscopy was carried out in an ultra high vacuum apparatus with a base pressure of 5×10^{-9} Pa [15]. All XPS measurements were performed at room temperature. The UHV apparatus is equipped with a preparation chamber, containing an Ar^+ sputter gun for additional cleaning procedures.

XPS is performed using a hemispherical analyzer (VSW HA100) and a commercial non-monochromatic x-ray source (Specs RQ20/38C). During XPS, x-ray photons irradiate the surface under an angle of 80° to the surface normal, illuminating a spot with a diameter of several mm. For all measurements presented here, the Al K_α line (photon energy 1486.6 eV) is used. Electrons are recorded by the hemispherical analyzer with an energy resolution of 1.1 eV emitted under an angle of 10° to the surface normal.

The transmission function of the analyzer has been previously determined experimentally. All XPS measurements were corrected by this transmission function. XPS spectra are displayed as a function of binding energy with respect to the Fermi level.

For quantitative XPS analysis, photoelectron peak areas are calculated via mathematical fitting with Gauss-type profiles using OriginPro 7G including the PFM fitting module, which applies Levenberg–Marquardt algorithms to achieve the best agreement between experimental data and fit.

Photoelectric cross sections as calculated by Scofield [16] and inelastic mean free paths from the NIST database [17] as well as the energy-dependent transmission function of the hemispherical analyzer are taken into account when calculating stoichiometry.

Transmission electron microscopy (TEM) was done with an image corrected FEI Titan 80-300 microscope operated at 300 kV and equipped with Gatan Tridiem 963 energy filter and an EDAX S-UTW energy dispersive x-ray (EDX) detector. TEM cross-sectional sample preparation was done by in situ lift-out using an FEI Strata 400S focussed ion beam (FIB) with the final polishing performed at 5 kV. The samples were investigated in cross-sectional geometry using bright-field TEM (BF-TEM), dark-field TEM (DF-TEM), high resolution TEM (HR-TEM), selected area electron diffraction (SAED) and scanning TEM (STEM) with a high angle annular dark-fied (HAADF) in combination with energy dispersive x-ray analysis (EDX). In situ heating experiments were performed using the ProtoChips Aduro holder with resistive MEMS heating.

For the characterization of the crystallographic structure of the films, the samples were analyzed by grazing incidence x-ray diffractometry (GIXRD). Using GIXRD, the x-rays strike the sample under a small angle. The detector is moved while the sample is kept fixed. Because of the small incident angle maximum information from the film is obtained while Bragg peaks from the substrate can be eliminated. We worked with a Bruker D5000 diffractometer using Co K_α radiation ($\lambda = 0.1789$ nm, 40 kV, 40 mA). A rocking curve was recorded before each GIXRD measurement to eliminate a possible tilt angle of the sample. The grazing incidence angle was 5°. At this angle, the substrate did not contribute to the diffractograms, and a maximum count rate from the film was achieved.

The surface topography of the as-deposited Si_2C and the annealed Si_2C surfaces is determined by atomic force microscopy (AFM) using a Veeco Dimension 3100 SPM. All measurements are performed in tapping mode with Al-coated silicon cantilevers (NSC15, Micromasch). The typical resonant frequencies of this series are about 325 kHz, typical spring constants are in the range of 40 N/m. The radius of the tip curvature is less than 10 nm. All images consist of 512 lines each containing 512 pixels. They are recorded with line-scan frequencies of 0.25–1.0 Hz. SPIP (Image Metrology A/S) is used for the depiction of the AFM images and the calculation of the average surface roughness (RMS) according to ISO 4287/1.

SEM was carried out in a scanning auger electron microscope (Omicron NanoSAM) with a base pressure below 10^{-8} Pa. The spatial resolution of 5 nm for Auger electron spectroscopy mode and about 3 nm in SEM mode is suitable for the characterization of small structures. All SEM images were taken with a primary electron energy of 5 keV.

3. Results and discussion

3.1. XPS fitting procedure

For a better understanding of the fitting procedure which we used for all our XPS spectra, the reader is referred to Fig. 1. It shows representative fits of the Si2p and C1s core level spectra and the corresponding relations between the different species, which have been considered. Literature studies as well as own reference measurements were used to work out a reliable fitting algorithm. The corresponding fit parameters are summarized in Table 1. Considering the tetrahedron model of amorphous silicon carbide introduced by K. Mui and F. W. Smith [11], the Si2p spectra were fitted with several components assigned to homonuclear Si-Si, heteronuclear Si-C and a mixture of Si-Si-C bonds. Besides, there are two more peaks representing O-Si-C and Si-O. The C1s spectra consist of at least two different peaks corresponding to C-Si and C-C bonds. Additional species could be identified as C-O and C=O. The distance between the C-Si and the Si-C peak was held constant at 182.1 eV and was previously experimentally determined along with the full width at half maximum (FWHM) of the corresponding peaks from a SiC (111) single crystal (Mateck GmbH, Germany). Subsequently, the FWHM of the Si-Si peak as well as the distance to the Si-O were determined from a Si (100) single crystal (CrysTec GmbH, Germany). The energetic distances between the other species shown in Fig. 1 are based on several values taken from literature [18–22]. These values are unfortunately quite different, which means that a distinct assignment of the individual species is difficult. By comparison of various publications concerning this topic and by persistent testing of the parameters, we agree on the values listed in Table 1. The FWHM of the species which were not experimentally determinable were fixed on appropriate values for all measurement.

3.2. As-deposited Si_2C

The results of XPS, AFM and GIXRD measurements of the as-deposited Si_2C film were published recently [13] and will therefore only be summarized here. The as-deposited sample contains a variety of bonding states consisting of homonuclear Si-Si, mixed Si-Si-C and heteronuclear Si-C bonds, where the major contributions were attributed to Si-Si and non-stoichiometric Si-Si-C. Furthermore, the film

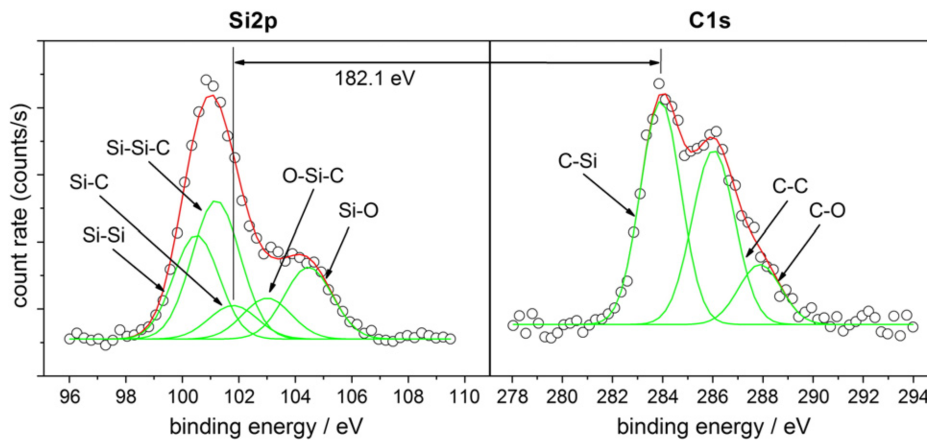

Fig. 1. Illustration of the XPS fitting procedure. The spectra show generic fits of the Si2p and C1s core levels and the corresponding assignment to different bonding species.

showed a smooth surface with an RMS roughness smaller than 1 nm and was entirely amorphous.

In addition to these results, TEM results of the as-prepared film are shown in Fig. 2. HAADF-STEM, HR-TEM images and the corresponding fast Fourier transform (FFT) pattern reveal the presence of a homogeneous amorphous film on a single crystalline Si substrate with smooth interfaces. Some isolated pores with diameters of about 100 nm can be found sporadically at the Si_2C/Si interface. A phase separation into Si and SiC_x rich regions was not observed.

3.3. Si_2C films annealed at 1200 °C for 2 h

The XPS results for Si_2C annealed at 1200 °C for 2 h are shown in Fig. 3. The XPS survey spectrum in Fig. 3a exhibits the same elemental peaks as obtained for the untreated sample. The sample contains 40% silicon, 27% carbon and 33% oxygen at the surface, resulting in a Si/C ratio of 1.5. Thus, the global elemental composition of the film remained nearly unchanged. However, the annealing procedure affected the bonding structure of the amorphous Si_2C layer, as indicated by the Si2p and C1s detail spectra in Figs. 3b and 3c. The amount of the mixed Si-Si-C bonding states vanished. Only Si-Si, Si-C and O-Si-C and SiO_2 are detectable. The oxide is attributed to a thin oxide layer on the surface of the film (see below). The C1s spectrum shows the well-known C-Si bonding state but also a large amount of C-C, C-O and C=O species. All XPS data-like binding energies, peak widths and the relative intensities of the corresponding species are summarized in Table 1.

The GIXRD results are depicted in Fig. 4. In addition, the diffractograms of an as-deposited film are also shown. In the GIXRD patterns. peaks at 55.5° and 41.6° are detectable, corresponding to the Si (220) and SiC (111) reflex, respectively. This indicates the crystallization of silicon and silicon carbide in the film during thermal annealing.

The rearrangement in the bonding structure and the crystallization process involves a distinct change in surface topography, as verified by AFM in Fig. 5. The image shows large but smooth structures of 500–600 nm height and 2–2.5 μm in diameter. The comparatively smooth areas between those structures may represent the remaining surface of the film.

Corresponding TEM images are shown in Fig. 6. The main part of the film is porous with oxidized layers at the surface. A sequence of a SiO_2 layer (300 nm) and two different SiC_xO_y layers (10–100 nm for each) are identified by image analysis and corresponding EDX analysis. The chemical composition of the surface structure was determined by local EELS and EDX line profiles. Integration across the different regimes reveals the following approximate nominal composition (basic EDX quantification without thickness correction of reference materials for the calibration): $Si_{30}O_{70}$ (top layer), $Si_{28}C_{30}O_{42}$ (upper SiC_xO_y layer) and $Si_{52}O_{16}C_{32}$ (lower SiC_xO_y layer), respectively. This result indicates a step-wise reduction of oxygen activity between surface and film. The composition of the main Si_2C film was assessed to $Si_{56}O_9C_{35}$. Oxide formation is attributed to oxygen contaminations of the furnace atmosphere during annealing at 1200 °C.

The film is composed of Si crystallites, 3C-SiC crystallites and pores all in the range of several tens of nm. The existence of some residual amorphous phase cannot be excluded. HAADF-STEM shows that phase separation and pore formation occur at a smaller length scale at the top of the film compared to the bottom (interface). BF- and DF-TEM images taken at different positions of the film do not show significant

Table 1
Relative distance (*) and peak width (FWHM) of the various Si2p and C1s species that were used in the XPS fitting algorithm as well as binding energy (BE), peak width and relative intensity of the Si2p and C1s species of the Si_2C sample annealed at 1200 °C for 2 h and 20 h, respectively.

	Si2p					C1s			
XPS fitting algorithm	Si-Si	Si-Si-C	Si-C	O-Si-C	Si-O	C-Si	C-C	C-O	C=O
ΔE/eV	*	0.7	1.3	2.5	3.8	*	1.9–2.1	3.9	–
FWHM/eV	1.9	2.0	2.0	2.0	2.0	1.9	2.0	2.0	–
1200 °C 2 h	Si-Si	Si-Si-C	Si-C	O-Si-C	Si-O	C-Si	C-C	C-O	C=O
BE/eV	100.5	101.2	101.8	103.0	104.3	283.9	286.0	287.8	290.2
FWHM/eV	1.9	2.0	2.0	2.0	2.0	1.9	2.0	2.0	2.5
Relative Int.	0.56	0.00	0.16	0.13	0.15	0.36	0.41	0.12	0.11
1200 °C 20 h	Si-Si	Si-Si-C	Si-C	O-Si-C	Si-O	C-Si	C-C	C-O	C=O
BE/eV	–	–	102.3	103.5	104.8	284.4	286.5	288.3	–
FWHM/eV	–	–	2.0	2.0	2.0	1.9	2.0	2.0	–
Relative Int.	–	–	0.71	0.17	0.12	0.74	0.21	0.05	–

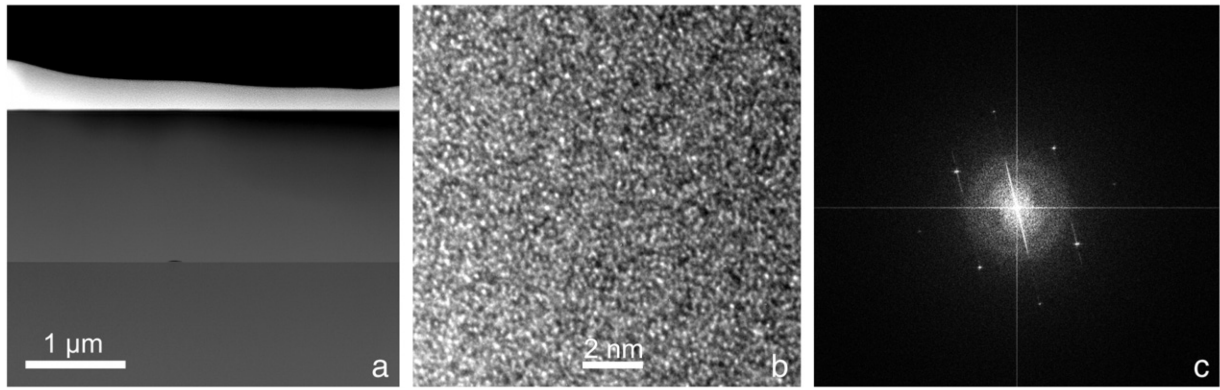

Fig. 2. HAADF-STEM (a) and HR-TEM (b) images in cross-sectional geometry of an as-deposited Si_2C film on Si substrate. The corresponding FFT pattern is shown in (c). The sharp reflexes correspond to the silicon substrate and the diffuse area to amorphous Si_2C. The amorphous nature of the film is obvious.

variations in crystallinity. At the Si substrate interface, a pore of about 1 μm thickness is found. This pore is located on a single crystalline silicon precipitate that is epitaxial grown on the substrate. In addition, further small Si crystallites are found at the substrate interface by HRTEM. This result illustrates that silicon is transferred from the Si_2C film matrix to the substrate interface during annealing. The surface structures already identified by AFM are also visible in the TEM picture. The humps are composed of SiO_2 and seem to be correlated with the existence of the pore and the epitaxial Si growth at the Si_2C/Si interface. This finding is confirmed for other FIB lamella.

3.4. Si_2C films annealed at 1200 °C for 20 h

Fig. 7 shows the XPS results for the Si_2C sample annealed at 1200 °C for 20 h. Only silicon, carbon, oxygen and molybdenum from the sample holder could be found, similar to the samples shown above. However, the chemical composition of the film has changed. The stoichiometry contains 39% silicon, 42% carbon and 19% oxygen. Thus, the Si/C ratio amounts to 0.9. This value is quite smaller compared to the untreated sample and to the sample which was annealed for 2 h. In addition, the oxygen content in the film decreased. The XPS detail spectra are

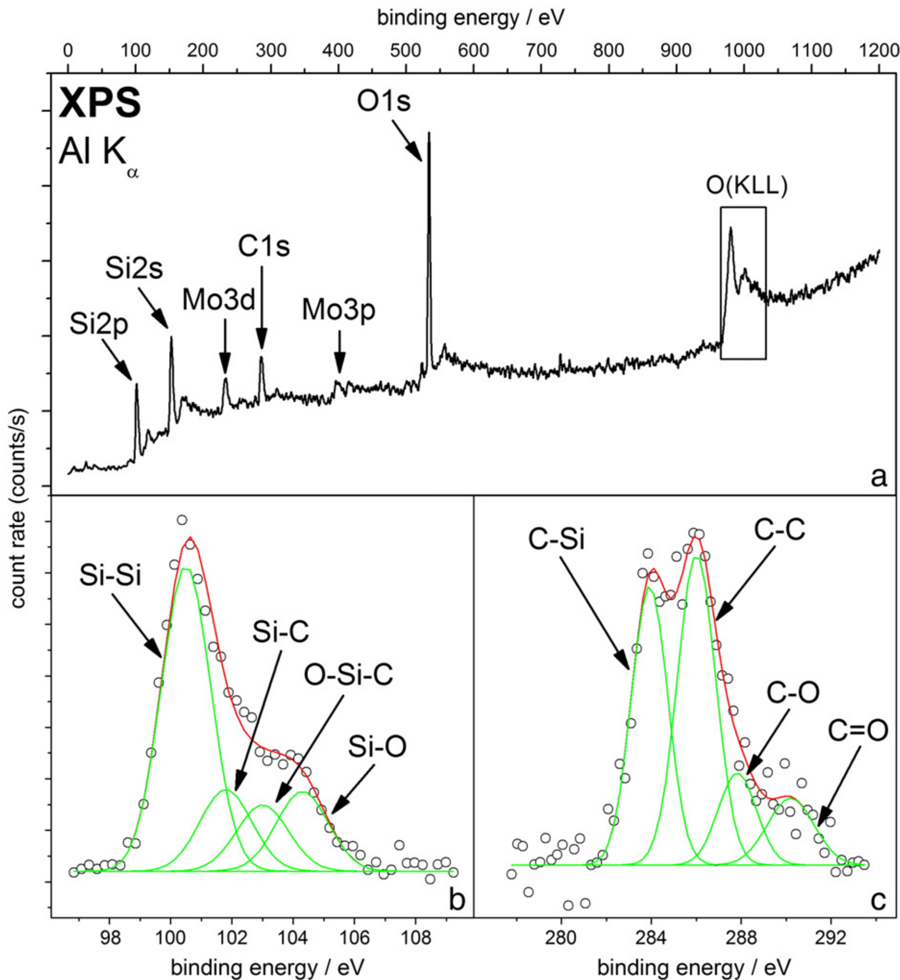

Fig. 3. XPS survey (a) and detail spectra (Si2p b, C1s c) of Si_2C annealed at 1200 °C for 2 h. The annealing procedure affected the bonding structure compared to the as-deposited sample.

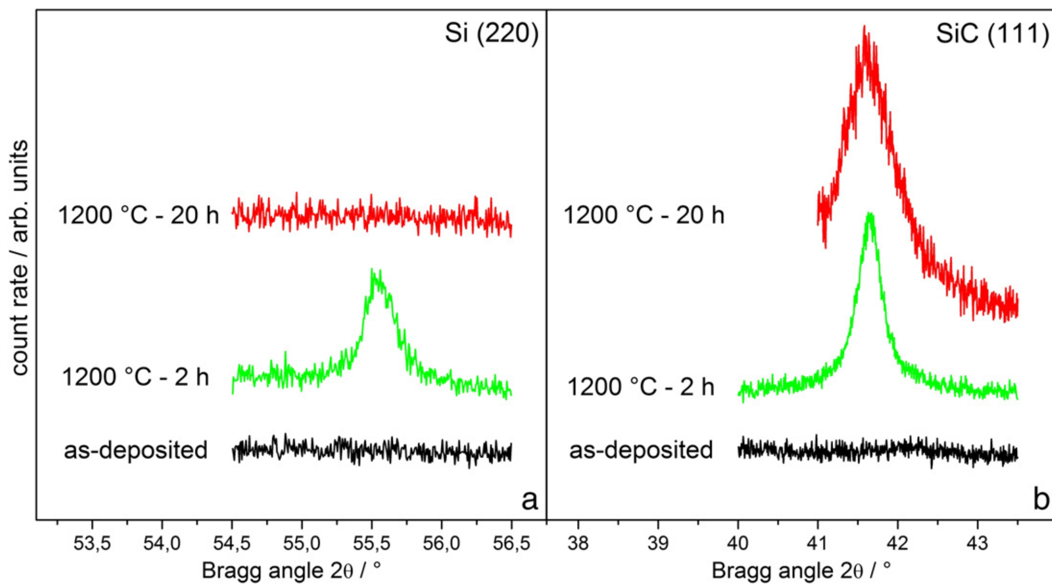

Fig. 4. GIXRD diffractograms in the range of the characteristic Si (220) and SiC (111) Bragg reflexes for the as-deposited and the annealed samples. The vanishing of the Si peak for long annealing times is clearly shown.

depicted in Figs. 7b and 7c. The Si2p spectrum shows Si-C, O-Si-C and SiO_2 bonding states. We were not able to fit this spectrum assuming an Si-Si bonding state, which indicates that there is no homonuclear Si bonding in the surface region of the film. The C1s spectrum contains C-Si and a $_{\text{variety}}$ of other species like C-C and C-O. Compared to the sample annealed at 1200 °C for 2 h the amount of these non-Si-bonded carbon species is considerably smaller. All XPS data-like binding energies, peak widths and the relative intensities of the corresponding species are summarized in Table 1. The disappearance of Si-Si bonding, verified by XPS, suggests that no crystallized or amorphous silicon exists within the detection depth of XPS (several nm).

The lack of polycrystalline silicon within the whole Si_2C film is proven GIXRD, as shown in Fig. 4. For the sample annealed at 1200 °C for 20 h, there is still a peak at around 41.6°, corresponding to the SiC (111) Bragg reflex, but no indication of crystallized silicon, represented by the Si (220) reflex at 55.5°.

Thus, the silicon, crystallized during thermal annealing at 1200 °C for 2 h, vanished after a period of 20 h. To get a closer look on the topographical changes, Fig. 8 shows an AFM image of the sample. Large structures of 400–500 nm height and several μm in diameter are visible,

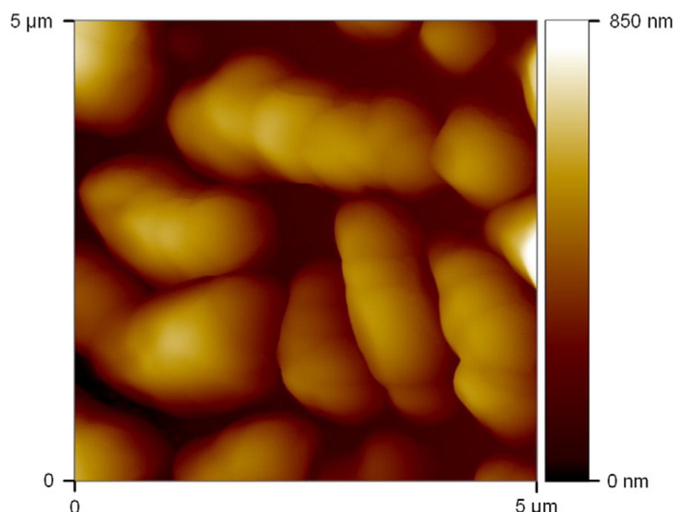

Fig. 5. AFM image of Si_2C annealed at 1200 °C for 2 h. After annealing a rough surface with large structures is revealed.

similar to the sample annealed for 2 h. However, the smooth surface of these structures changed to a very jagged structure. In addition to AFM, we also used SEM to get a high resolution image of the surface. The according SEM image is depicted in Fig. 9. It shows large-scale, jagged structures similar to AFM, broken by vast areas of a flat but porous subsurface. Investigations with TEM and SAED on a sample annealed for very long times of 120 h confirmed the presence of SiC nanocrystallites and the complete lack of silicon.

3.5. Additional in situ TEM studies on Si_2C films annealed at 1000 °C

For a further insight into the crystallization behavior, additional in situ TEM studies were launched at 1000 °C in a vacuum of about 0.1 mPa. The lower temperature compared to the bulk measurements is due to technical reasons. However, we expect that the TEM analysis is a good reference for elucidating the starting point of phase separation and initial crystallization. Fig. 10 shows BF-TEM images and corresponding SAED patterns after heating an FIB lamella to 1000 °C in the TEM microscope for 1, 3 and 4 min. After annealing the initial amorphous Si_2C film (Figs. 10a and 10d) for only 1 min (Figs. 10b and 10e), large-density variations become visible and the main diffraction peaks in SAED correspond to SiC and low-intensity Si powder rings appear in the SAED pattern. This indicates a nano-crystalline SiC structure with some additional polycrystalline Si, in accordance with the ex situ measurements. Prolonged annealing for 3 and 4 min (Figs. 10f and 10g) leads to the formation of large area silicon crystals on the Si_2C layer. Fig. 10c shows a real space image of the later stage of the heating process (4 min). At a first glance, it looks similar to the previous stages, but on top of everything is a very large grain thin Si film, which is, e.g., filling the crack on the top-right side of the image. In the SAED pattern after 4 min of annealing (Fig. 10g), the presence of a thin almost single crystalline Si film is confirmed, which spreads across the whole TEM lamella with the nanocrystalline SiC underneath.

3.6. Discussion

Obviously, thermal annealing of amorphous Si_2C at 1200 °C between 2 and 20 h is accompanied by two fundamental processes: (i) the crystallization of silicon and stoichiometric silicon carbide and (ii) the disappearance of any crystallized silicon afterwards in GIXRD and XPS measurements. Concerning the first point, at 1200 °C, the temperature

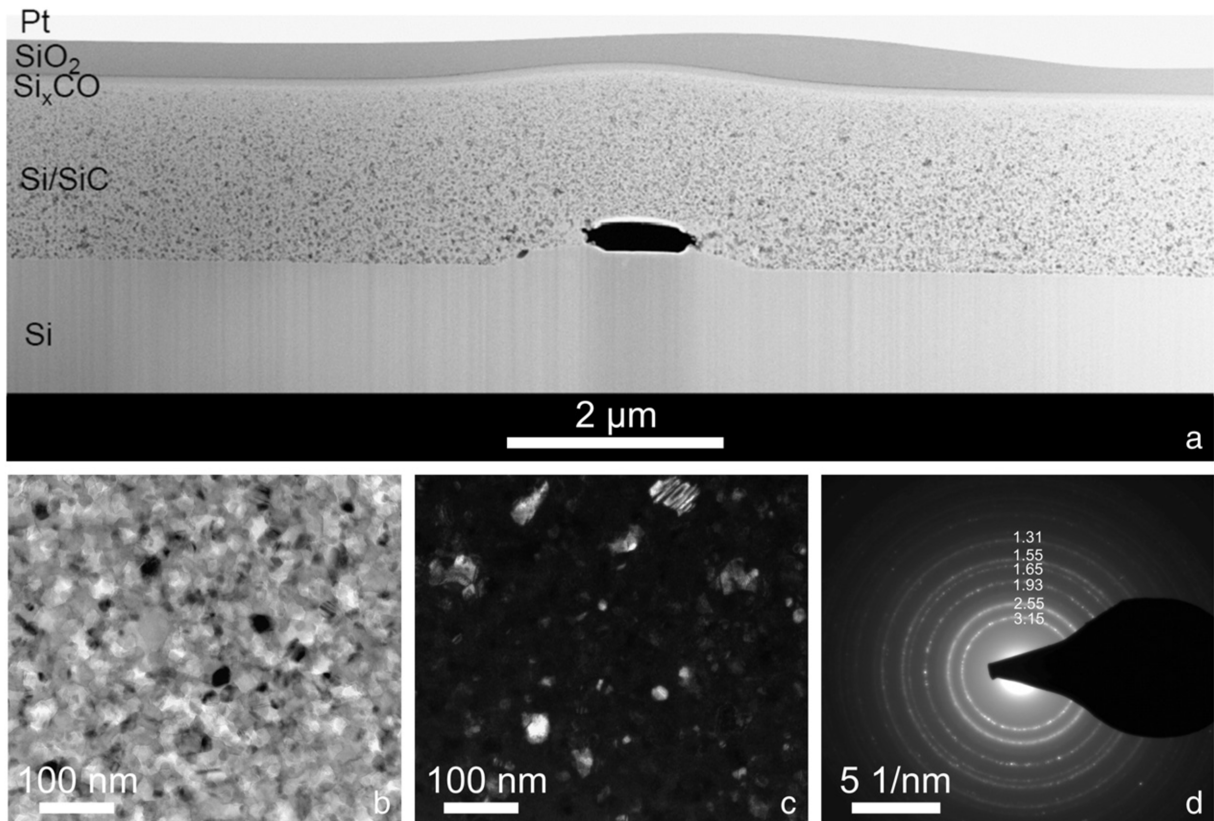

Fig. 6. HAADF-STEM overview image of the film treated at 1200 °C for 2 h in cross-sectional geometry (a). BF-TEM (b) and DF-TEM (c) images of the film as well as the corresponding SAED pattern (d) are given. The nano-crystalline structure and the surficial oxide layers are visible.

is apparently high enough for the crystallization of Si and SiC as seen above, which is consistent with similar observations reported in literature [23,24]. With regard to the difference in bonding energy between Si-Si (1.81 eV [25]) and Si-C (4.47 eV [26]), the phase transformation starts most probably with the predominant break of homonuclear Si-Si bonds. Particularly in the case of a silicon-rich amorphous film like Si_2C, there will also be a variety of unbound or weakly bound silicon atoms due to geometric considerations. The high temperature enhances the Si diffusion, which allows the Si atoms to increasingly build up new Si-C bonds with the dangling bonds of partially bonded carbon atoms and also to agglomerate to Si clusters. Afterwards, both type of phases crystallize with short annealing times in the range of minutes. The in situ TEM studies indicate a slightly retarded crystallization of silicon compared to SiC.

The vanishing of polycrystalline silicon during annealing is quite hard to understand at first sight. The ex situ TEM investigations at 1200 °C (2 h) as well as the in situ TEM investigations at 1000 °C (some minutes) indicate that silicon diffuses out of the film to the surface or substrate interface, where it segregates in form of large single crystals or epitaxially on the Si substrate. In this state, it can no longer be detected by GIXRD experiments. Because of the special geometry of such experiments, GIXRD is sensitive to randomly oriented polycrystalline material only and not to single crystals misoriented with respect to the present reflection condition. The apparent loss of silicon and the significant decrease in the Si/C ratio as found by XPS (within the spatial detection range) has to be due to the relatively fast diffusion at this temperature, which enables the migration of silicon atoms to one of the interfaces. The high diffusivity of Si already at 1000 °C could be directly seen in the in situ TEM experiments, where Si quickly diffused out of the TEM lamella to form a thin large single crystalline silicon film on the surface. In the bulk specimen, the transport path might be along the surface of the pores, found by TEM analysis, and/or along grain boundaries in the partially crystallized structure. In this context three processes are conceivable:

I diffusion to the substrate and subsequent epitaxial growth of silicon at the Si_2C/Si interface,
II diffusion to the surface of the Si_2C film and subsequent formation of large Si crystals at UV conditions or alternatively sublimation of silicon [28] and
III diffusion to the surface of the Si_2C film and subsequent formation of SiO_2 in an Argon atmosphere with residual oxygen in the percent range.

The last point would also explain the comparatively thick SiO_2 layer (or SiO_xC_y layer) at the surface, if one considers the transformation of Si to SiO_2 by the reaction with oxygen contaminations in the Ar atmosphere. At 1200 °C, oxygen molecules are able to diffuse through the SiO_2 layer and to react at the interface with free silicon.

However, the question concerning the driving force for the apparent diffusion of Si atoms to the interfaces during thermal annealing is still without reply. Most probably, the answer lies in geometric constraints. To illustrate this, let us first consider a stoichiometric amorphous SiC film and clarify what could be the driving force for chemical ordering. In this context, J. Tersoff identified two crucial factors [27]: the chemical preference of Si-C bonding and the geometric constraints. The latter is based on differences in atomic sizes and bond lengths of the involved species. This creates a large amount of local stress in the material. In contrast to the crystal phase, an amorphous structure is able to accommodate most of the local strain. However, in crystallized SiC, local strain plays an important role and thus a homogenous distribution of Si-C bonds is energetically favourable. That is the reason why, beneath thermodynamic reasons, thermal annealing of amorphous stoichiometric SiC finally leads to the crystallization of SiC and not to a phase separated mixture of Si, C and SiC.

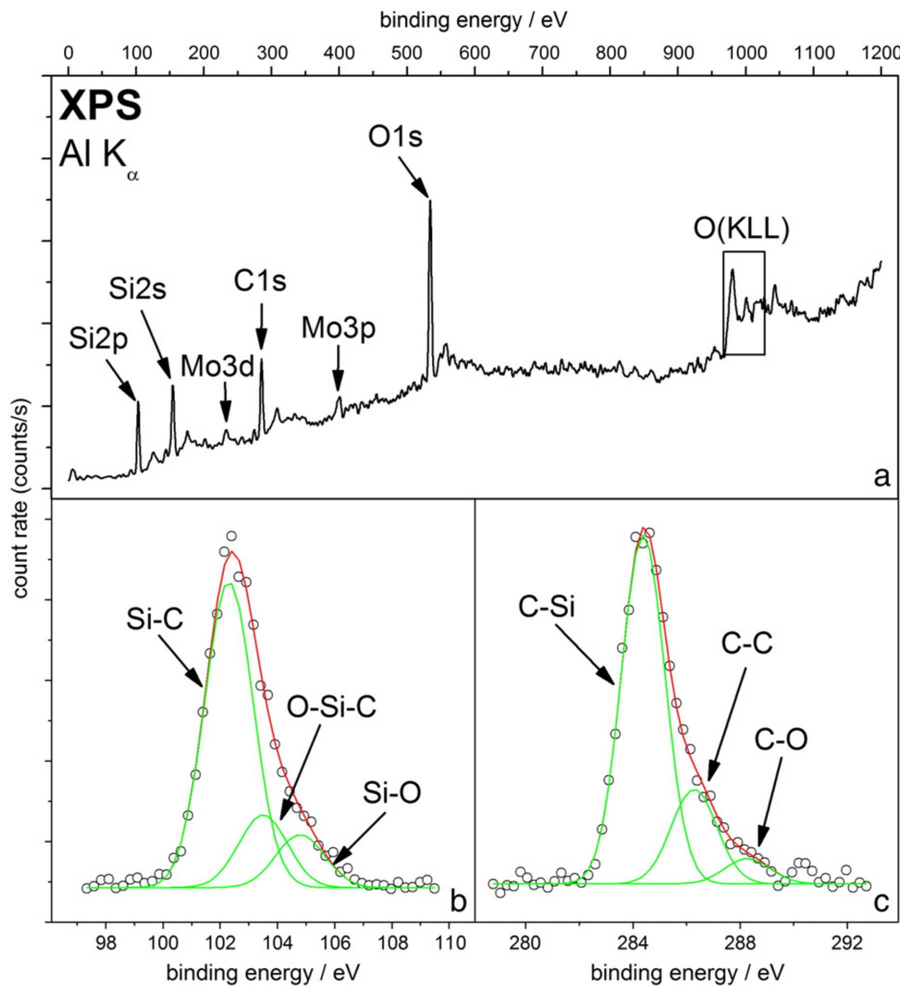

Fig. 7. XPS survey (a) and detail spectra (Si2p b, C1s c) of Si_2C annealed at 1200 °C for 20 h. The amount of Si-Si bonds has completely vanished.

Now we can assume that the same geometric constraints that force the chemical order in crystallized stoichiometric SiC are responsible for the disappearance of crystallized silicon in the present case. The difference between stoichiometric and silicon-rich amorphous silicon carbide is the fact that the amorphous phase exhibits a variety of unbound silicon atoms due to the break of homonuclear Si-Si bonds mentioned above and that the silicon still crystallizes in the early stage of the thermal annealing process. In the very early stage of crystallization, a nanostructure composed of a still amorphous matrix and phase separated nanocrystalline SiC and Si is present. Hence, local strain is small. If crystallization proceeds, additional SiC is formed and SiC grain growth takes place, which results in coarser grained crystallites. Local stress can no

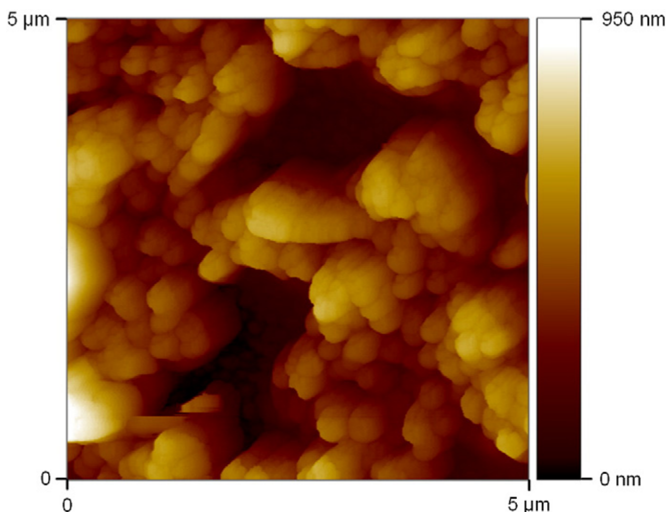

Fig. 8. AFM image of Si_2C annealed at 1200 °C for 20 h. The surface roughness has changed dramatically.

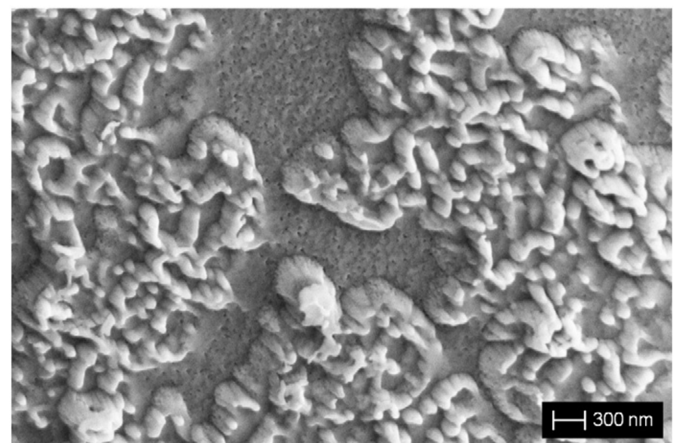

Fig. 9. SEM image of Si_2C annealed at 1200 °C for 20 h. The image shows a very jagged and porous surface.

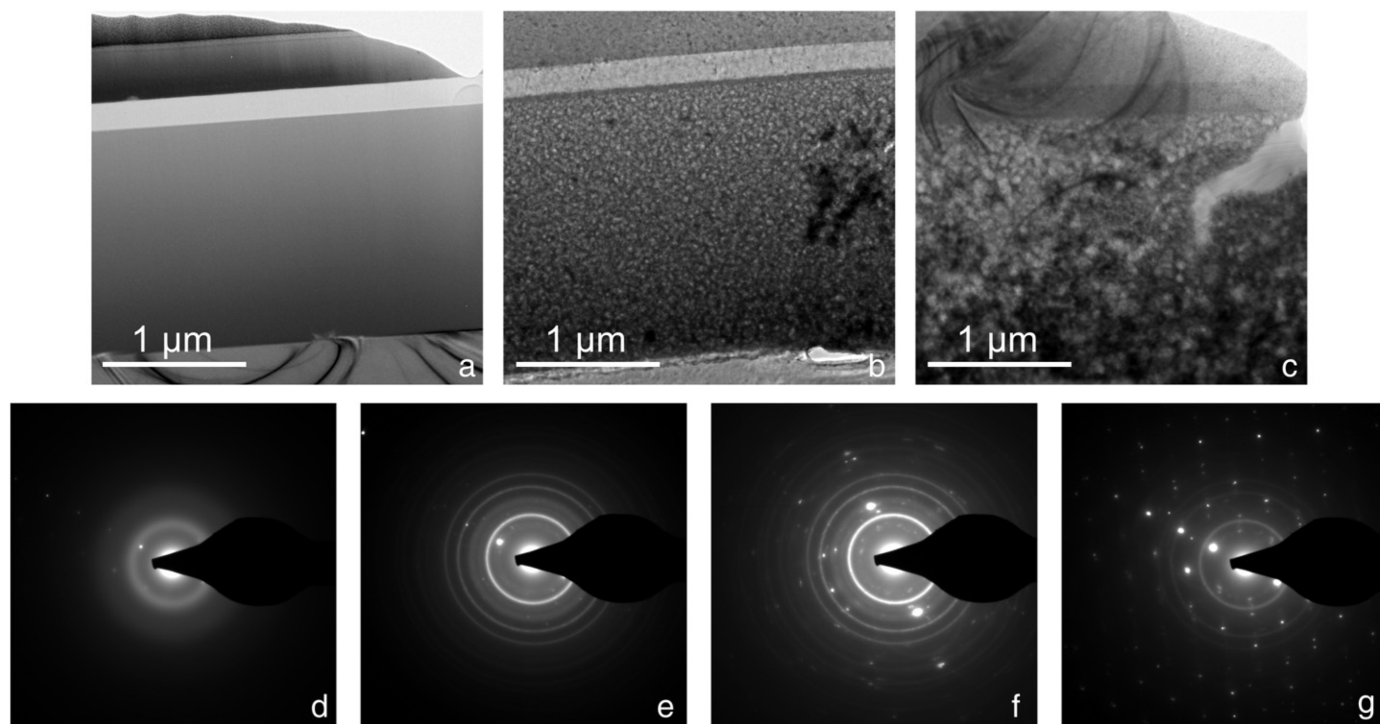

Fig. 10. BF-TEM images taken during in situ annealing at 1000 °C in cross-sectional geometry for the as-deposited sample (a), and the same sample annealed for 1 min (b) and for 4 min (c), respectively. Corresponding SAED images of the film in the as-deposited state (d), after 1 min of annealing (e), after 3 min of annealing (f) and after 4 min of annealing (g) at 1000 °C. The structural evolution and the formation of crystalline SiC and Si are illustrated.

longer be properly accommodated. In combination with the small binding energy of Si-Si bonds and the chemical preference of Si-C bonding, local stress will force the decomposition of the crystallized silicon phase and the diffusion to interfaces. The assumption that stress plays a considerable role is supported by the fact that during the crystallization at 1200 °C, significant microstrain is formed with increasing annealing time as found by a Williamson Hall analysis of XRD data in [15]. In addition, during annealing at 1200 °C, a significant growth of the SiC crystallites takes place [15], which can be seen as a coarsening process in the later stages. This might be an additional factor of a geometric constraint that forces silicon to diffuse to the interfaces. The growing SiC crystallites "squeeze" the silicon out of the structural arrangement of the film.

4. Summary

In this study, we investigated the thermal stability of amorphous Si_2C thin films, deposited on silicon substrates at high temperatures. The samples were annealed at 1200 °C in a resistance tube furnace for 2 and 20 h, respectively, and afterwards analyzed by means of XPS, ex situ and in situ TEM GIXRD, AFM and SEM. Annealing at 1200 °C is accompanied by a significant change in the bonding structure and the surface topography of the film. Annealing for 2 h led to the crystallization of silicon and silicon carbide and to the formation of large structures at the surface. After 20 h of thermal annealing, the entire crystallized silicon disappeared and the surface exhibits jagged and porous structures. We tried to explain our observations by developing a model considering a number of processes involved: (i) agglomeration of silicon in the amorphous phase in the early stage of annealing, (ii) subsequent crystallization of silicon carbide and silicon and (iii) decomposition of the crystallized silicon and diffusion of silicon to the interfaces. We further suppose that the driving force for the decomposition of the entire crystallized silicon can be traced back to geometric constraints based on local strain in the material.

Acknowledgements

This research has been supported by the German Research Foundation (DFG) under the contract Schm1569/9-2. The authors would like to thank S. Korte and G. Lilienkamp for SEM measurements (Omicron NanoSAM provided by the German Research Foundation (DFG), grant number: INST 189/158-1) and S. Dahle for experimental assistance. We would further like to thank M. Bruns for his annotations according this paper and Prof. W. Daum for providing the AFM. This work was partially carried out with the support of the Karlsruhe Nano Micro Facility (KNMF), a Helmholtz Research Infrastructure at Karlsruhe Institute of Technology (KIT, www.kit.edu)

References

[1] G. Ambrosone, U. Coscia, S. Lettieri, P. Maddalena, C. Privato, S. Ferrero, Thin Solid Films 403–404 (2002) 349.
[2] J. Bullot, M.P. Schmidt, Phys. Status Solidi B 143 (1987) 345.
[3] F. Alvarez, L.R. Tessler, Solid State Phenom. 44–46 (1995) 3.
[4] G. Foti, Appl. Surf. Sci. 184 (2001) 20.
[5] W.A. Nevin, H. Yamagishi, M. Yamaguchi, Y. Tawada, Nature 368 (1994) 529.
[6] T. Ichihara, K. Aizawa, J. Non-Cryst. Solids 227–230 (1998) 1345.
[7] W.B. Xing, A.M. Wilson, K. Eguchi, G. Zank, J.R. Dahn, J. Electrochem. Soc. 144 (1997) 2410.
[8] C. Ricciardi, G. Fanchini, P. Mandracci, Diam. Relat. Mater. 12 (2003) 1236.
[9] Z. Wan, S. Huang, M.A. Green, G. Conibeer, Nano. Res. Lett. 6 (2011) 129.
[10] G.-R. Chang, F. Ma, D.-Y. Ma, K.-W. Xu, Nanotechnology 21 (2010) 465605.
[11] K. Mui, F.W. Smith, Phys. Rev. B 35 (1987) 8080.
[12] F. Finochhi, G. Galli, M. Parinello, C.M. Bertoni, Phys. Rev. Lett. 68 (1992) 3044.
[13] R. Gustus, W. Gruber, L. Wegewitz, H. Schmidt, W. Maus-Friedrichs, Appl. Surf. Sci. 258 (2012) 5567.
[14] W. Gruber, H. Hadjiamini Najafabadi, U. Geckle, M. Bruns, H. Schmidt, Philos. Mag. 90 (2010) 3855.
[15] M. Frerichs, F. Voigts, W. Maus-Friedrichs, Appl. Surf. Sci. 253 (2006) 950.
[16] J.H. Scofield, J. Electron Spectrosc. Relat. Phenom. 8 (1976) 129.
[17] http://www.nist.gov/srd/nist71.htm.
[18] T. Takeshita, Y. Kurata, S. Hasegawa, J. Appl. Phys. 71 (1992) 5395.
[19] K.V. Emtsev, Th. Seyller, F. Speck, L. Ley, P. Stojanov, J.D. Riley, R.G.C. Leckey, Mater. Sci. Forum 556–557 (2007) 525.
[20] P. Mélinon, P. Kéghélian, A. Perez, C. Ray, J. Lermé, M. Pellarin, M. Broyer, M. Boudeulle, B. Champagnon, J.L. Rousset, Phys. Rev. B 58 (1998) 16481.

[21] S. Kerdiles, R. Rizk, A. Pérez-Rodríguez, B. Garrido, O. González-Varona, L. Calvo-Barrio, J.R. Morante, Solid State Electron. 42 (1998) 2315.
[22] Naoto Kikushi, Eiji Kusano, Tatsuya Tanaka, Akira Kinbara, Hidehito Nanto, Surf. Coat. Technol. 149 (2002) 76.
[23] A.M. Hartel, M. Künle, P. Löper, S. Janz, A.W. Bett, Sol. Energy Mater. Sol. Cells 94 (2010) 1942.
[24] Y. Wang, J. Lin, C.H.A. Huan, Z.C. Feng, S.J. Chua, Thin Solid Films 384 (2001) 173.
[25] Q.Y. Tong, K. Gutjahr, S. Hopfe, U. Gösele, Appl. Phys. Lett. 70 (1997) 1390.
[26] K. Zellama, P. Germain, S. Squelard, J.C. Bourgoin, J. Appl. Phys. 50 (1979) 6995.
[27] J. Tersoff, Phys. Rev. B 49 (1994) 16349.
[28] W.A. de Heer, C. Berger, M. Ruan, M. Sprinkle, X. Li, Y. Hu, B. Zhang, J. Hankinson, E. Conrad, Proc. Natl. Acad. Sci. U. S. A. 108 (2011) 16900.